Space Sci Rev (2017) 211:501–524
DOI 10.1007/s11214-017-0378-0

Modeling of Ground Deformation and Shallow Surface Waves Generated by Martian Dust Devils and Perspectives for Near-Surface Structure Inversion

Balthasar Kenda[1] · Philippe Lognonné[1] · Aymeric Spiga[2] · Taichi Kawamura[1] · Sharon Kedar[3] · William Bruce Banerdt[3] · Ralph Lorenz[4] · Don Banfield[5] · Matthew Golombek[3]

Received: 5 September 2016 / Accepted: 8 May 2017 / Published online: 14 June 2017

Abstract We investigated the possible seismic signatures of dust devils on Mars, both at long and short period, based on the analysis of Earth data and on forward modeling for Mars. Seismic and meteorological data collected in the Mojave Desert, California, recorded the signals generated by dust devils. In the 10–100 s band, the quasi-static surface deformation triggered by pressure fluctuations resulted in detectable ground-tilt effects: these are in good agreement with our modeling based on Sorrells' theory. In addition, high-frequency records also exhibit a significant excitation in correspondence to dust devil episodes. Besides wind noise, this signal includes shallow surface waves due to the atmosphere-surface coupling and is used for a preliminary inversion of the near-surface S-wave profile down to 50 m depth. In the case of Mars, we modeled the long-period signals generated by the pressure field resulting from turbulence-resolving Large-Eddy Simulations. For typical dust-devil-like vortices with pressure drops of a couple Pascals, the corresponding horizontal acceleration is of a few nm/s^2 for rocky subsurface models and reaches 10–20 nm/s^2 for weak regolith models. In both cases, this signal can be detected by the Very-Broad Band seismometers of the InSight/SEIS experiment up to a distance of a few hundred meters from the vortex, the amplitude of the signal decreasing as the inverse of the distance. Atmospheric vortices are thus expected to be detected at the InSight landing site; the analysis of their

Electronic supplementary material The online version of this article (doi:10.1007/s11214-017-0378-0) contains supplementary material, which is available to authorized users.

✉ B. Kenda
kenda@ipgp.fr

1 Institut de Physique du Globe de Paris, Sorbonne Paris Cité, UMR 7154 CNRS, Univ. Paris Diderot, 75013 Paris, France

2 Laboratoire de Météorologie Dynamique, UMR CNRS 8539, Institut Pierre-Simon Laplace, UPMC Univ. Paris 6, Sorbonne Universités, 4 Place Jussieu, 75005 Paris, France

3 Jet Propulsion Laboratory, California Institute of Technology, 4800 Oak Grove Drive, Pasadena 91109, CA, USA

4 Johns Hopkins University Applied Physics Laboratory, 11100 Johns Hopkins Road, Laurel, MD 20723, USA

5 Cornell Univeristy, Ithaca, NY 14853, USA

seismic and atmospheric signals could lead to additional constraints on the near-surface structure, more precisely on the ground compliance and possibly on the seismic velocities.

Keywords Dust devils · Mars · Ground tilt · Subsurface · Large-eddy simulation · Insight

1 Introduction

Dust devils are small-scale atmospheric vortices made visible by the entrainment of dust particles: their detection and their analysis are therefore simpler than in the case of non dust-laden vortices. The development of these convective vortices is associated with Planetary Boundary Layer (PBL) convection driven by solar heating of the surface; moreover visible dust devils form if loose material is available to be lifted from the surface. These conditions occur typically in arid areas on Earth and in many regions of Mars. The first detection of dust devils on Mars dates back to the Viking mission (Ryan and Lucich 1986), but their existence and contribution to the atmospheric dust content had been proposed even earlier (Neubauer 1966). In the following decades, orbital and surface observations resulted in remote and in situ detections of Martian dust devils, leading to a characterization of their dynamics, of their frequency and of their impact on the Mars atmosphere; for a historical perspective on the subject, we refer to the review by Lorenz et al. (2016).

Most meteorological parameters undergo characteristic abrupt fluctuations during the passage of convective vortices: surface pressure drop, temperature increase, rapid changes in the wind direction, as well as a quasi-electrostatic and a magnetic field when charged dust particles are transported. All these fluctuations have been observed on Earth (Rennó et al. 2004; Farrell et al. 2004; Lorenz 2012) and on Mars (Schofield et al. 1997; Kahanpää et al. 2004), except for electrostatic and magnetic detections in the case of Mars. These measurements provided constraints for modeling, from idealized thermodynamical estimates (Rennó et al. 2000) to turbulence-resolving numerical simulations (see Spiga et al. 2016 for a review).

In addition to their atmospheric signature, atmospheric vortices also generate seismic signals, which may be used for constraining the subsurface (Lognonné and Johnson 2007). At long period, i.e. for $T > 10$ s, the perturbation of the surface pressure field induces a quasi-static ground deformation. In weak soils, the vertical displacement can be large enough to generate detectable tilt effects, as recently shown by a terrestrial field experiment on a dry lakebed (Lorenz et al. 2015). At high frequency, $f > 1$ Hz, dust devils generate acoustic waves in the infrasound band (Schmitter 2010; Lorenz and Christie 2015) and we will show in this paper they are also a source of short-period Rayleigh waves. The distance to the source can therefore be determined by differential travel time measurements between the air wave and the Rayleigh surface wave, when both propagation velocities are known, and the sources can furthermore be localized with both the records of the azimuth of the seismic signals and the track left by the vortex. Dust devils can therefore be considered natural and free active seismic sources that may prove useful for probing the shallow subsurface. Note that from a seismological perspective it is not important whether a vortex is dust-laden or not: the expected signals are indeed caused by the pressure fluctuation and by the turbulent wind field. This leads sometimes to semantic confusion, referring to "dust devils" rather than to their corresponding pressure fluctuations.

The 2018 InSight mission to Mars will deploy a single seismic station on the surface of the planet. The seismometer of the Seismic Experiment for Interior Structure (SEIS) is designed to study the interior of the planet through the signals generated by the seismic activity

of Mars (see Lognonné and Pike (2015) for a short description of the SEIS performance). But like all seismic sensors, the seismometer will also record the ground motion caused by the atmosphere-solid planet coupling; Mimoun et al. (2017) developed a general noise models for Mars including atmospheric contributions, whereas Murdoch et al. (2017a) focused on the wind-induced mechanical noise on the InSight Lander.

Convective cells and turbulent vortices induce pressure changes that deform the surface and can act as seismic sources. This leads to static ground deformation at long periods and to the generation of seismic waves at short periods, both potentially hiding seismic signals caused by quakes or meteor impacts. At long period, careful corrections for the atmospheric contribution are thus necessary in order to remove the effect of static loading and improve the signal to noise ratio (Beauduin et al. 1996; Zürn et al. 2007). Murdoch et al. (2017b) estimated the background-noise level based on Large-Eddy Simulations (LES) and discussed the efficiency of pressure-decorellation methods. At short period, the only way to reduce the wind-induced noise on a low-velocity surface layer is to bury the sensors down to the bedrock (Withers et al. 1996; Naderyan et al. 2016). Nevertheless, these excitations can also be viewed as interesting seismic signals constraining both the atmospheric activity of the PBL and the subsurface structure. The aim of this work is to model and characterize the various seismic signals produced by atmospheric vortices, investigate whether they could be detected on Mars and propose preliminary inversion strategies for the near surface based on these signals. To do this, we first review the theoretical basis of the ground deformation induced by pressure loading and of the propagation of shallow surface waves. We then analyze Earth data showing how these techniques can be applied to vortices. Finally we model the vortex-induced signals on Mars using the realistic pressure field derived from LES and discuss the resulting prospects for detection and the capabilities of a single station analysis.

2 Theoretical Background

Local atmospheric turbulence generates ground deformation and ground displacements that can be divided into two main categories: long-period ground quasi-static deformation caused by local surface-pressure fluctuations and wind-shear stresses and shallow high-frequency ground vibrations associated to surface waves excited regionally by turbulent phenomena, and more generally by the high-frequency part of the pressure and wind turbulence.

These turbulences, as well as the pressure singularities like dust devils, are most of the time observed when a background wind drives the local atmospheric circulation, especially during daytime on Mars, when they are the most active. Both the pressure fluctuations in the vortex (or dust devil) and the displacement with the background wind of these fluctuation concur to the overall pressure forces and pressure force gradient applied to the ground.

A model of the signature of turbulences and dust devils requires to couple the surface pressure field, provided by LES or by measurements of the pressure field, with the elastic response of the near surface. This, like all elastic methods, can be made by different approaches, depending on the strategy used for the computation of space gradient. Both finite differences, spectral methods or Green's functions summation can therefore be used. In the spectral domain, however, the environment wind is concentrating the energy of the pressure field time variations along the apparent wave number of the wind, which for a given frequency of the signal, will be expressed as $k = \frac{\omega}{c}$, where ω is the angular frequency and c the wind velocity. If the pressure drop of a dust devil is a relatively constant feature in time and depends mostly on the distance toward the center, most of the space gradient of the time dependent pressure wave will therefore be controlled by the background wind. On

the other hand, if the pressure drop is generating high frequency fluctuations, the source in frequency domain will be an amplitude modulation of a propagating wave controlled by the background wind. Of course, for any more complex field, the complete elastic response can be obtained if the pressure field is decomposed into an infinite number of plane waves (e.g. for spectral methods) or point sources (e.g. for Green's function summations). The acoustic and the high-frequency seismic signatures of atmospheric vortices, including tornadoes and dust devils, constitute a much more complex subject, as the sources can be not only at the surface but also in the atmosphere, due to infrasound/seismic wave conversions: the appropriate theoretical description is still controversial and the available terrestrial data are not completely consistent with one of the several proposed models (see e.g. Bedard 2005; Howe 2002; Tatom et al. 1995). Moreover, at high frequency the ambient wind contributes to generate a background noise (Withers et al. 1996; Mucciarelli et al. 2005) trapped in the upper layers, between the bedrock and the surface, which acts as a waveguide. This makes the precise identification of localized atmospheric sources challenging and the noise results more from the activity of the entire Planetary Boundary Layer in the vicinity of the lander.

A full forward modeling of the high-frequency excitation is thus complex and beyond the scope of this work. We focus instead on the analysis of available terrestrial data and we limit the theoretical discussion to the dispersion of shallow Rayleigh waves in a stratified medium.

2.1 Long-Period Ground Motion

The classical method to compute the long-period ground deformation induced by pressure fluctuation carried by background wind is Sorrells' Theory. The approximation proposed by Sorrells (1971) and Sorrells et al. (1971) assumes that the pressure disturbances propagate at the ambient wind speed c and can therefore be represented as plane waves $e^{i(\omega t - kx)}$ modulated in amplitude by the pressure fluctuation and where the wavenumber k depends on the angular frequency ω via the formula $k = \omega/c$. Thanks to this relation, the simple elastostatic formulation results in a dynamical description: the ground sensitivity to surface loading can thus be expressed in terms of frequency and wind speed.

We adapted the Sorrells et al. (1971) framework to horizontally layered subsurface models by developing a Thomson-Haskell type matrix formulation of the elastostatic equation. We include two end-member, one-dimensional subsurface models developed from the characterization of the landing site using remote sensing data and the geological processes that formed it (Golombek et al. 2017). Surface materials are dominated by cohesionless to slightly cohesive sand size particles produced by impact and aeolian activity. Laboratory tests of simulants that encompass the material properties derived from the landing site evaluation have been subjected to laboratory tests to derive their elastic properties (Delage et al. 2017). The first model assumes a thick deposit of cohesionless sand and consists of a half space that has low density and low seismic velocities. The second model includes the same fine-grained regolith (sand) that grades into coarse breccia overlying fractured bedrock at 20 m depth (Golombek et al. 2017; Warner et al. 2017) and is similar to the model of Knapmeyer-Endrun et al. (2017) that is derived from laboratory tests (e.g., Delage et al. 2017), elastic properties models (Kedar et al. 2017), and observations of subsurface properties of an aeolian surface layer over a rubble zone that grades into lava flows in the Cima volcanic field of the Mojave Desert. This model has progressively increasing seismic velocities and density with depth. The assumed properties for these two models is shown in Fig. 1.

The resulting sensitivity profiles (Fig. 2) show typical values in the range of 2–20 nm/Pa for the vertical sensitivity R_v at long period (10–100 s); horizontal sensitivities R_h are

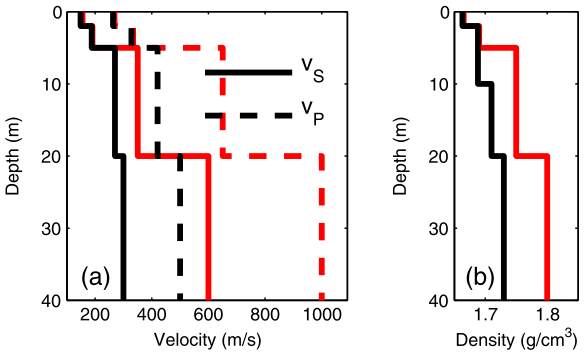

Fig. 1 Elastic properties of two reference 1D models of the Mars subsurface. Pure regolith halfspace (*black*) and regolith layer over fractured bedrock (*red*): P-wave (v_P) and S-wave (v_S) velocities (**a**) and density (**b**) profiles

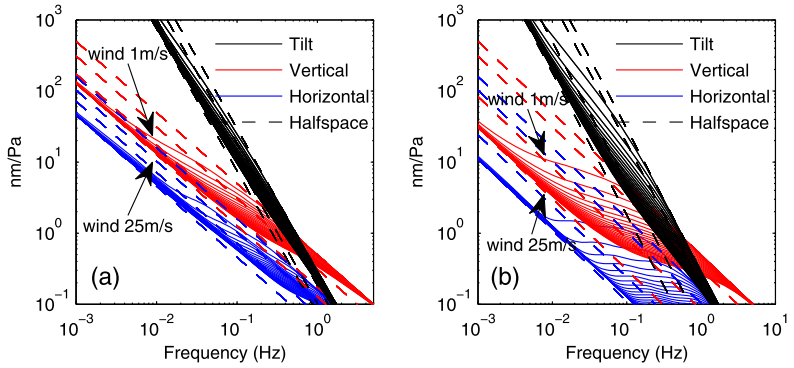

Fig. 2 Ground sensitivity to static loading. (**a**) is for the regolith model, (**b**) for the fractured bedrock; tilt equivalent displacement (*black*), vertical (*red*) and horizontal (*blue*) sensitivities are shown. The successive dashed lines correspond to the halfspace models with the velocities of the successive layers, whereas each continuous line corresponds to an increasing wind velocity in the range 1–25 m/s. At short period, only the shallow layer is seen, whereas the sensitivity is converging to the one of the deepest layer at long period

smaller by a factor of 5–10 in this frequency band. However, on the horizontal component the tilt effect dominates for periods longer than 1 s, and it becomes even larger than vertical displacement for periods above 5 s. To compare the tilt acceleration with the horizontal and vertical displacement, we computed the apparent horizontal displacement due to ground tilt following Sorrells (1971). Moreover, it should be noted that the ground sensitivity does not depend directly upon the seismic velocities, but on the bulk and shear moduli of the medium (see Sorrells 1971; Sorrells et al. 1971 for the complete derivation of the ground sensitivities).

Sorrells' approach is a particularly useful approximation, especially when single-point pressure time series are available and when the background wind speed and direction are known or can be estimated. This will be the case for the InSight seismic and meteorological measurements, thanks to the Auxiliary Payload Sensor Suite (APSS), which will be equipped with wind sensors and an extremely sensitive microbarometer. Moreover, in the hypothesis of a homogeneous half-space, the formulation is even simpler and directly relates pressure fluctuation, vertical velocity and ground tilt. In particular, for each sinusoidal component of the pressure field, P_{ω_0} the vertical displacement, w, the horizontal displacement, u and the tilt acceleration T at the surface are given in terms of the pressure fluctuation by (Sorrells 1971, Equations 24, 25, 26 and 27)

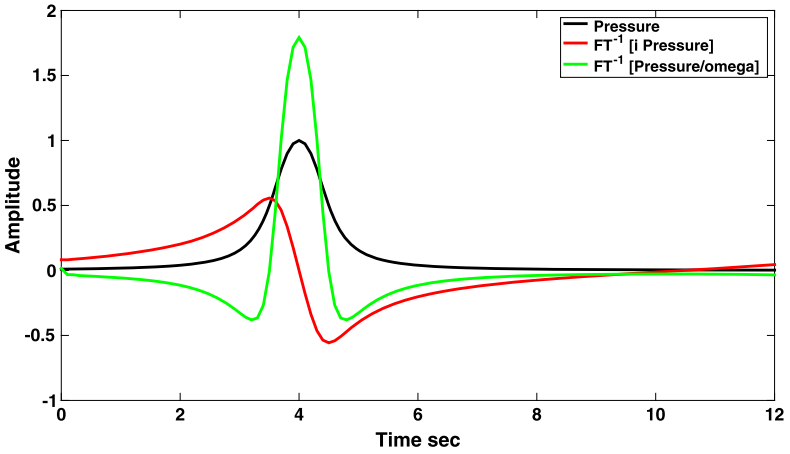

Fig. 3 Example of ground acceleration and tilt response for a simple pressure signal. The pressure model is the one proposed by Vatistas et al. (1991) with $\Delta P(x) = [1 - (2/\pi)\arctan(r^2)]$, with $r = 2x/D$, $D = 5$ m and with a traveling velocity of $c = 5$ m/s and passing on a the measurement point at 4 s. The two transformed pressure functions used in Sorrells' expressions are shown in red for iP, associated to the tilt and ωP for the vertical acceleration

$$w = -\frac{c_0(\lambda + 2\mu)}{2\mu(\lambda + \mu)} \frac{P_{\omega_0}}{\omega_0}, \tag{1}$$

$$u = \frac{ic_0}{2(\lambda + \mu)} \frac{P_{\omega_0}}{\omega_0}, \tag{2}$$

$$T = ig \frac{\lambda + 2\mu}{2\mu(\lambda + \mu)} P_{\omega_0}, \tag{3}$$

where c_0 is the wind speed, g is surface gravity, λ and μ the elastic parameters, and ω_0 the angular frequency. Figure 3 illustrates, for a typical dust devil pressure drop used by Lorenz (2014), the typical characteristic shapes which can be encountered on the horizontal axis, through tilt, and on the vertical axis.

Substituting P_{ω_0} from Equation 1 into Equation 2 and passing to the frequency domain, we get the relation

$$\frac{T + u\omega^2}{g} \frac{1}{1 + \omega \frac{c\mu}{g(\lambda+2\mu)}} = -\frac{\dot{w}}{c}, \tag{4}$$

where a dot denotes derivation with respect to time. At 50 s period on Earth and for winds of 5 m/s, $1 + \omega \frac{c\mu}{g(\lambda+2\mu)} \simeq 1$, and the horizontal component is then mainly due to ground tilt, and moreover it will also be proportional to the vertical ground velocity times $-g/c$. This property will be retrieved on Earth observations of dust devils in Sect. 3.1.

In order to obtain a reliable model of the signals generated by complex atmospheric structures like vortices, the Sorrells' hypothesis is not the most suitable, as it considers only the plane waves in the $\omega - k$ space along the observed wind direction. But the Sorrells' solution is the one for the spectral component $k = \frac{\omega}{c}$ and the generalization for all k components of the spectral pressure field is trivial. This more precise computation of the ground motion is then equivalent to pseudo-spectral methods and can be performed whenever a 2D surface-pressure field is available. In this case, the pressure field $P(x, y, t)$ can be transformed into its spectral components $\hat{P}(k_x, k_y, \omega)$, where a hat denotes the Fourier Transform. Each component associated to ground deformation is computed following Sor-

rells' approach, with the only difference that the norm of the wavevector, $|k| = (k_x^2 + k_y^2)^{0.5}$ is used instead of the plane-wave approximation $k = \frac{\omega}{c}$. The computation is performed in the frequency-wavenumber domain and the displacement at the surface is obtained by inverse Fourier Transform as follows:

$$\begin{cases} u(x,y,t) = \iiint \frac{k_x}{\sqrt{k_x^2+k_y^2}} R_h \hat{P}(\omega,k_x,k_y) e^{i(\omega t - k_x x - k_y y)} \mathrm{d}k_x \mathrm{d}k_y \mathrm{d}\omega \\ v(x,y,t) = \iiint \frac{k_y}{\sqrt{k_x^2+k_y^2}} R_h \hat{P}(\omega,k_x,k_y) e^{i(\omega t - k_x x - k_y y)} \mathrm{d}k_x \mathrm{d}k_y \mathrm{d}\omega \\ w(x,y,t) = \iiint R_v \hat{P}(\omega,k_x,k_y) e^{i(\omega t - k_x x - k_y y)} \mathrm{d}k_x \mathrm{d}k_y \mathrm{d}\omega. \end{cases} \tag{5}$$

Here u, v and w are the displacements in the x, y and z directions, respectively, z being directed upward. The acceleration effectively detected by a seismometer is the sum of the real ground acceleration and of the gravity perturbation induced by the displacement. The latter term includes the free-air anomaly on the vertical component and the tilt effect on the horizontal ones: for the small displacements involved here, a first-order approximation results in the following formula for the detected acceleration $\bar{a}$, r being the radius of the planet:

$$\begin{cases} a_x = -\ddot{u} + g\frac{\partial w}{\partial x} \\ a_y = -\ddot{v} + g\frac{\partial w}{\partial y} \\ a_z = -\ddot{w} + 2g\frac{w}{r}. \end{cases} \tag{6}$$

Concerning the vertical component of Equation 6, the comparison of the inertial and free-air anomaly terms shows that the latter becomes dominant whenever

$$2g\frac{w}{r} > \ddot{w} = 4\pi^2 f^2 w, \tag{7}$$

where f is frequency, that is for

$$f < \sqrt{\frac{g}{2\pi r}}. \tag{8}$$

It follows that the free-air anomaly on Mars is equal or larger than the real ground acceleration for frequencies below 0.23 mHz (compared to 0.28 mHz for the Earth), and is thus significant for tidal analysis.

A complementary approach focused on the background tilt experienced by a single seismic station is discussed in Murdoch et al. (2017b). In that work, the ground displacement and the related tilt are computed through Green's functions for a purely regolith halfspace with homogeneous properties and using the same reference pressure model as in this paper; for a cross-validation of these two approaches based on the comparison of the results for the same structural model and excitation source see Murdoch et al. (2017b). Both Sorrell's theory and the more precise spectral or Green's function methods may be used, once seismic data are available and the atmospheric source is known (through direct measurements and additional data such as dust devil track) to estimate ground properties, mainly the compliance and possibly its frequency-dependence, which leads to the layering.

2.2 Shallow Surface Waves

Short-period surface waves are sensitive to the shallow layers of the subsurface: indeed the penetration depth of Rayleigh waves scales as the wavelength. In the frequency band 1–20 Hz and for the low S-wave velocities significant for Mars, this depth can be estimated to vary from a few meters to a few tens of meters, which explains why the amplitude of these

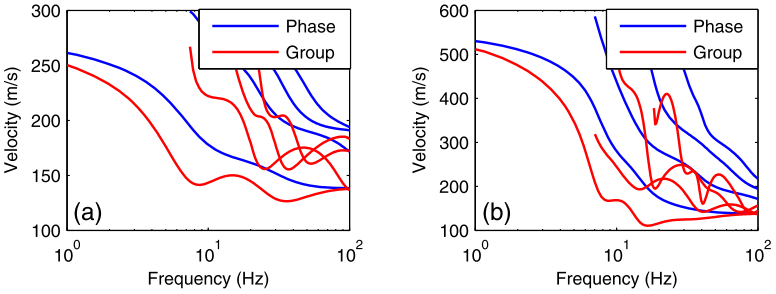

Fig. 4 Rayleigh-wave dispersion in the subsurface of Mars. The fundamental mode and the first three overtones are shown for the regolith model (**a**) and for the fractured-bedrock model (**b**)

trapped surface waves decay very rapidly with depth. This is one of the main reasons for burying short periods sensors in order to achieve low wind noise sensitivity (e.g. Withers et al. 1996). In addition, one of the other main features of surface waves in horizontally layered media is that they are dispersive, i.e. the propagation velocity depends on the frequency. Computations of the Rayleigh-wave dispersion for the two reference subsurface models are shown in Fig. 4. The curves were computed through Herrmann's Computer Programs in Seismology (Herrmann 2013), which solve the elastodynamic equation in layered media via a matrix propagator method.

For the models under consideration, the dispersion of the fundamental Rayleigh mode is mainly concentrated in the 1–20 Hz band: the analysis of this frequency band is thus crucial in the exploration of the near surface. Moreover, the layering of the subsurface is responsible for the presence of local extrema in the dispersion of the group velocity, called Airy's phases (Fig. 4, red curves). Since the energy is transported at the group velocity and the Airy's phases are non-dispersive, the energy itself is expected to concentrate around these frequencies (Kennet 1983; Ritzwoller and Levshin 2002). The analysis of short-period waves excited by atmospheric turbulence, as well as of background noise, should therefore evidence these non-dispersive phases and provide additional useful information for the inversion of the seismic velocities down to a few tens of meters depth. The dispersion curves, and in particular the Airy's phases, strongly depend on the actual structure of the subsurface at the landing site, which is unknown, even if constrained by geology (Golombek et al. 2017) and experiments with simulants (Delage et al. 2017). The two presented model are realistic examples and they also constitute two limit cases; in both cases, and for a larger class of models in between these two, a common feature is that the Rayleigh wave dispersion of the fundamental and of the first overtones, lies mainly between 1 and 20 Hz. Regardless of the precise values of the seismic velocities and of the non-dispersive frequencies, we thus expect the 1–20 Hz band to be significant for this analysis.

3 Terrestrial Observations and Inversion

The field experiment carried out by Lorenz et al. (2015) in the Mojave Desert (California) resulted in the seismometer detection of dust devils by ground tilt. The near-surface structure being known, the authors modeled the ground tilt by means of a simple single-point loading approach.

We propose here a more refined modeling of the long-period excitation based on Sorrells' Theory. Moreover, seismic and pressure data were sampled at 100 counts/s: we can thus

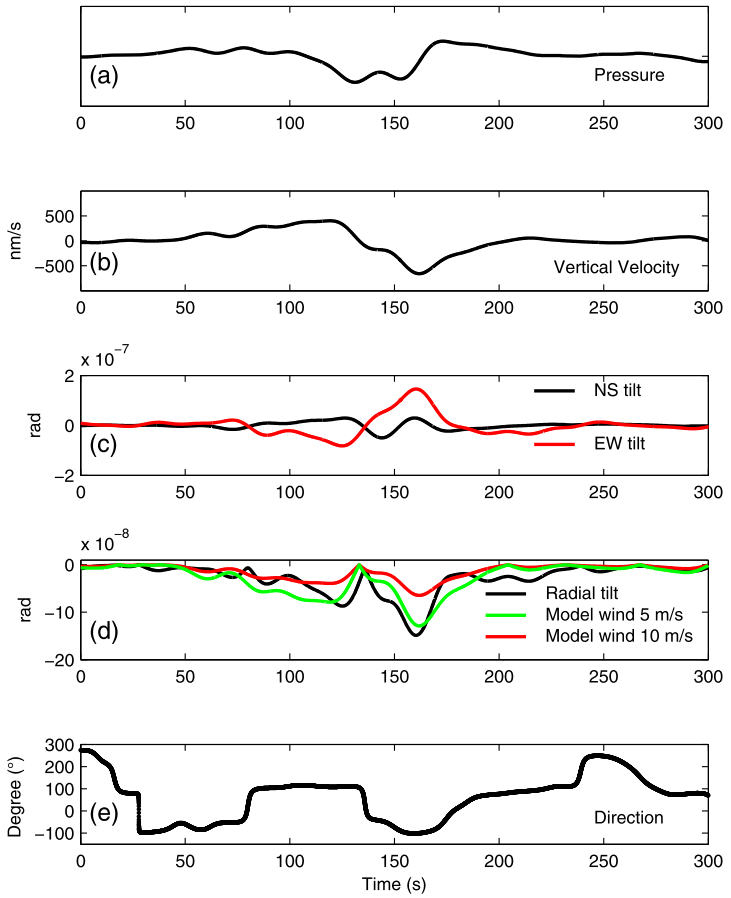

Fig. 5 Long-period time history of a dust devil episode recorded in the Mojave Desert, California. (**a**) Pressure fluctuation obtained by integration of the microbarometer data. (**b**) Vertical velocity filtered in the 20–100 s band. (**c**) Tilt in the NS and EW direction derived from horizontal accelerations low-pass filtered at 20 s. (**d**) Amplitude of the radial tilt: measured (*black*) and modeled for wind speed at 5 m/s (*green*) and 10 m/s (*red*). (**e**) Apparent wind direction inferred from tilt azimuth indicating a possible cycloidal migration of the vortex

perform a first study of the high-frequency content of the signal and apply spectral analysis for a preliminary inversion attempt.

3.1 Ground Tilt

The long-period seismic signals of two dust devil episodes were identified by Lorenz et al. (2015) on the horizontal components and interpreted as the ground tilt induced by the pressure fluctuation. For the first episode, the signature of the vortex appears also in the time series of the pressure and of the vertical velocity (Figs. 5a and 5b), the latter being not reported in Lorenz et al. (2015).

A major difference between Earth and Mars observations will be not only the smaller strength of the dust devils but also the measurement noise at long period. Instead of using the raw, non filtered data shown by Lorenz et al. (2015), we focus on the 20–100 s periods

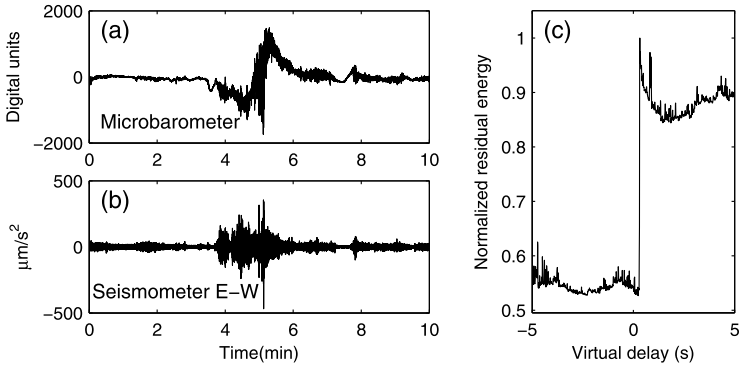

Fig. 6 Record of a terrestrial dust devil at 100 samples/s. Raw pressure (**a**) and seismic (**b**) time series. (**c**) Energy content of the seismic signal after pressure deconvolution, as a function of a virtual delay in the arrival time of the pressure signal

bandwidth, which is expected to be the best with respect to thermal noise during day time (e.g. Lognonné et al. 1996; Mimoun et al. 2017).

One way to test whether the local tilt can or not be approximated by the one induced by the background wind is to test Equation 4 for the recorded tilt and vertical displacement. Since the wind speed is unknown, we computed the amplitude of the expected radial tilt for two realistic wind conditions, i.e. 5 and 10 m/s, finding a good agreement with the measured tilt for a wind speed of 5 m/s (Fig. 5d). We emphasize that this agreement suggests how Sorrells' theory may be used also in the case of atmospheric vortices, even if here we did not directly derived the seismic signals from the pressure fluctuation, since the absolute value of the latter was not determined (Lorenz et al. 2015). More results on the difficult problem of retrieving tilt fluctuations from single-station measurements of the pressure (e.g. Zürn et al. 2007) in the case of Mars are presented in Murdoch et al. (2017b) and in Sect. 4 of this paper.

In addition to the amplitude of the tilt effect, its azimuth carries information about the position of the source: at each time, the dust devil is expected to be in the direction opposite to the measured tilt. This supplementary information permitted us to establish the direction of migration of the vortex (Fig. 5e). The time history of the apparent direction shows two abrupt changes during the passage of the vortex at 80 s and 135 s, and a smoother one at 180 s, which are compatible with a cycloidal trajectory. In this interpretation, the time interval of 50 s multiplied by a wind speed of 5 m/s, suggest an influence region of the vortex of about 250 m across. These rapid changes in the wind direction can explain the direction of the measured tilt, and not only its absolute value. An alternative interpretation accounting for the waveform of the radial tilt is a vortex passing right over the seismometer. Other abrupt direction changes appear in Fig. 5e, at about 25 s and 235 s, however since they occur when the measured tilt accelerations are very low, they are most likely not representative of the migration of the pressure field.

3.2 Acoustic and Surface Waves

No short period analysis was performed in the data of Lorenz et al. (2015) in order to search additional seismic signal associated to shallow structure surface waves, excited by the dust devil vortex but recorded remotely by the seismometer. For the first dust devil episode, the high-frequency seismic records show a significant rise in the noise level (Fig. 6a). A priori,

this increase could be related simply to stronger winds; to exclude this case and explore possible signatures of shallow surface waves, we analyzed the spectral properties of pressure and seismic records and compared them to synthetic surface wave velocities and dispersion for the same reference subsurface model used by Lorenz et al. (2015).

If a dust devil generates both infrasound and high-frequency seismic signals, a difference in the arrival times should be detected given the distinct propagation velocities of the waves. We looked for this difference in the acoustic and horizontal seismic data in the E-W direction, i.e. the direction of migration of the dust devil. Due to the proximity of the source, the expected delay is small, of the order of 0.1–0.5 s. The manual choice of the arrival times would therefore strongly affect the results; for this reason we proceeded with a sliding window pressure-deconvolution method and we analyzed the energy content of the residual seismic signal as a function of a virtual delay time (Fig. 6c). We computed this residual energy content instead of classical cross-correlation since there is no phase coherency between acoustic and seismic signal and therefore this method ensures a better estimation of the delay. As expected, a delay of the acoustic wave with respect to the seismic ones is measured: the discontinuity in the residual energy content for a virtual delay of 0.3 s indicates indeed this value as the actual delay Δt. The latter is related to the speed of sound c, to the Rayleigh-wave velocity v (since we are considering the longitudinal component), and to the distance to the vortex d_S by the formula $\Delta t = d_S(\frac{1}{c} - \frac{1}{v})$. Estimates of the Rayleigh wave velocity for the fundamental mode below a few Hz resulting from Lorenz et al. (2015), are of about 700–800 m/s and give a distance to the dust devil of 180–200 m.

Once established that the high-frequency signals consists of shallow surface waves, we analyzed the spectral content of this signal to investigate the properties of the subsurface and focused our analysis on the resonances, by using two different techniques sensitive to the latter.

The first one is the Horizontal to Vertical Spectral Ratio (HVSR, or H/V), a well-known method for near-surface exploration, routinely used in the determination of the thickness of sediment layers and, more recently, for S-wave profile inversions (Arai and Tokimatsu 2004). The HVSR is defined by

$$HV(\omega) = \frac{|\hat{A}_V(\omega)|}{\sqrt{|\hat{A}_{H1}(\omega)|^2 + |\hat{A}_{H2}(\omega)|^2}}, \tag{9}$$

where $\hat{A}_V$, $\hat{A}_{H1}$ and $\hat{A}_{H2}$ are the Fourier spectra of the seismic records. In horizontally layered media, and especially in the case of a homogeneous layer over a half-space, $HV(\omega)$ shows a peak that corresponds to the fundamental frequency of the material, $f_0 = 0.25 v_S / h$, where h is the thickness of the first layer and v_S its shear-wave velocity (Malischewsky and Scherenbaum 2004). The normalized H/V spectral ratio exhibits the most pronounced peak is at 11.2 Hz (Fig. 7). With the thickness of the first layers as in Lorenz et al. (2015)—that is $h = 5.6$ m—this peak corresponds to a S-wave velocity of 250 m/s, very close to the value of 260 m/s estimated by Lorenz et al. (2015) based on an active seismic survey. Since the H/V peak provides one equation in two unknowns, it needs to be coupled to other constraints to retrieve either the depth of the first layer or its S-wave velocity.

The second method is based on the Airy's phases we identified in the dispersion curves computed for the reference subsurface model of the site. In the case of a localized source like an Earthquake, Airy's phases appear as pulses in the time domain, whereas in the case of moving or diffuse sources, like vortices and other atmospheric features, the Airy's phases may correspond to high-energy spectral lines during extended intervals. A similar idea was developed by Konno and Ohmachi (1998) for the H/V ratio peaks: in this work it is pointed

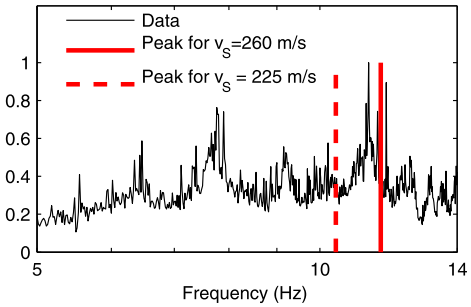

Fig. 7 Horizontal to vertical spectral ratio. Data from background noise are in *black* and frequencies of theoretical peaks for different values of the S-wave velocity in the first subsurface layer are in *red*

out how the peaks can be related to Rayleigh-wave ellipticity as well as to Airy's phases of the fundamental mode of the Love wave. Also Bonnefoy-Claudet et al. (1998) conclude that the H/V peak frequency could be explained, depending on the stratigraphical situation, by Rayleigh ellipticity, Love Airy's phases, S-wave resonance or a mix of them. Since the two cited works deal with the H/V ratio, they focused on Love waves, whereas we took into account the Airy's phases of Rayleigh waves and looked for a correspondence in the high-frequency seismic data. We thus compared the theoretical Airy's phases with the most excited frequencies appearing in the spectra of the background noise (Fig. 8b). Although other spectral peaks appear between f3 and f4, they are less pronounced compared to the surrounding ones and not well separated from another. A good agreement in the frequency band 2–20 Hz (Fig. 8c) encouraged us to develop a preliminary inversion attempt for the subsurface structure.

To develop a basic Monte Carlo inversion, we first computed the theoretical Airy's phases of Rayleigh waves (up to the fourth harmonic) varying the 1D subsurface structure for 10^5 models. Among these, we selected the acceptable models, i.e. the ones fitting the measured high-noise frequencies (illuminated in Fig. 8a). Since the selected peaks are not very sharp, we selected the fitting models by considering a 1Hz interval around the peaks of Fig. 8b. In this way we selected about 1800 different models coherent with the available measurements. For each value of a model parameter, its relative occurrence among the acceptable models constitutes an a posteriori estimate of its probability. The need for this kind of probabilistic Bayesian inversion follows from the high degree of degeneracy of the inverse problem. The resulting S-wave profile down to 50 m depth is shown in Fig. 9. Since the excited frequency bands identified in Fig. 8a are quite broad and the inverse problem itself is highly non-unique, the probability values are necessarily small and, correspondingly, the error bars large. Nevertheless the S-wave profile compares well with the three-layered reference model, especially in the depth range 25–50 m, whereas in the shallower layers the inversion appears to overestimate the S-wave velocity. This overestimation is likely related to the fact that we did not use in our inversion the high frequencies resonances above 15 Hz. However, the inversion is comparable in resolution to those made for other examples in planetary seismology, such as the subsurface inversions made on the Moon with the Apollo geophones (e.g. Larose et al. 2005).

4 Modeling for Mars

4.1 Large-Eddy Simulations

We now describe how the methodology developed in Sect. 3 for the terrestrial environment could be translated to Mars in order to assess the amplitude of the signals and the detec-

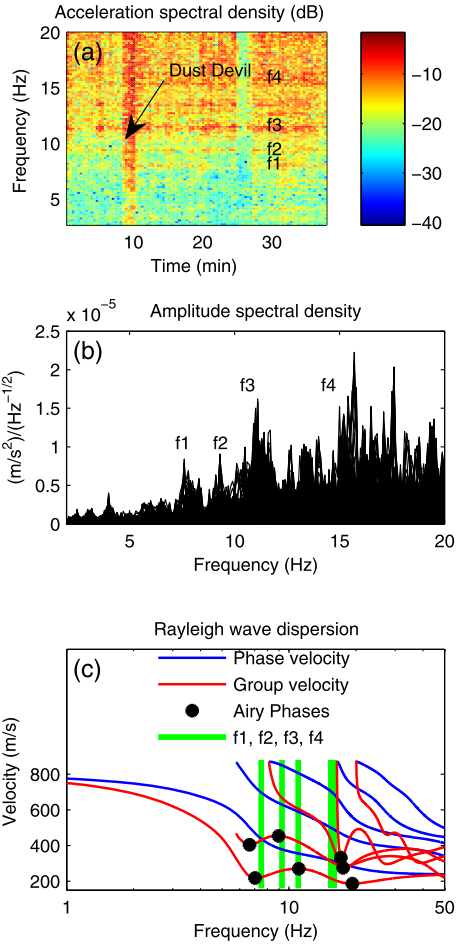

Fig. 8 Non-dispersive Airy's phases in the high-frequency part of the signal. (**a**) Spectrogram of dust devil episode and background noise, Airy's phases are denoted by $f_1 - f_4$. (**b**) Spectra of 100-s windows covering the 40-min record. (**c**) Forward modeling of the Rayleigh-wave dispersion curves (fundamental mode and four overtones) showing a comparison of predicted and measured Airy's phases

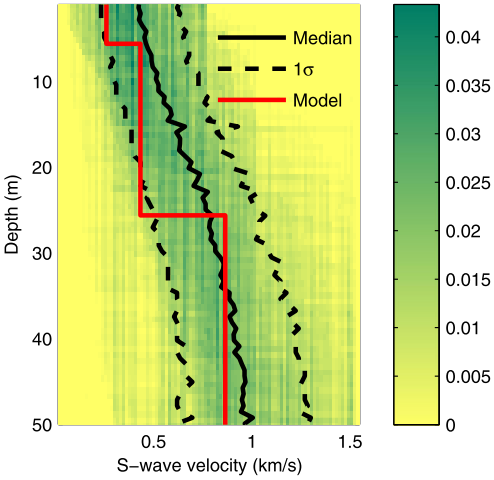

Fig. 9 S-wave velocity profile down to 50 m depth as resulting from the Monte Carlo inversion. The three-layered model of Lorenz et al. (2015) is represented by the *red line*, the median Monte Carlo profile and the 1σ interval by *black continuous* and *dashed curves*, respectively

tion perspectives for the InSight mission. Although the pressure noise on Mars has been estimated with the Sorrells' approach and with Viking's data at long period (Lognonné and Mosser 1993), no in-depth modeling has been made. A major limitation, which somewhat also stands for the Earth, is that the two-dimensional surface pressure field, necessary for all high resolution modeling of the ground displacement induced by turbulent events, is not observed with a spatial resolution suitable for the application of this formalism.

To overcome this caveat, and predict what could be the atmosphere-induced seismic signal on Mars, as well as potentially linking it to wind and temperature observations by the APSS module, we use the predictions of surface pressure from turbulent-resolving Large-Eddy Simulations. The basics of LES is to run a regional-scale model in idealized conditions (infinite and uniform flat plain terrain) at high resolution (< 200 m grid spacing) to resolve the largest turbulent eddies, responsible for Planetary Boundary Layer (PBL) mixing in afternoon convective conditions (Lilly 1962). Previous modeling studies showed that, in LES, the main features of the Martian daytime PBL are resolved: convective cells, turbulent plumes and convective vortices analogous to dust devils (e.g. Rafkin et al. 2001; Toigo et al. 2003; Michaels and Rafkin 2004; Spiga and Forget 2009).

The LES model employed here is described in details in Spiga et al. (2010), and combines a complete next-generation hydrodynamical solver (Skamarock and Klemp 2008) with physical parameterizations (notably radiative transfer) tailored for the Martian environment (Spiga and Forget 2009). The horizontal resolution in the LES carried out for this InSight study is 50 m as in Spiga et al. (2010), but we adopted a wider domain of 14.4 km across by using 289×289 grid points in the horizontal. The rationale for this choice is that observations in Hinson et al. (2008) for regions sharing similarities with the InSight landing site hint a daytime PBL about 4.5 km high. As detailed in Michaels and Rafkin (2004), who cite Mason (1989), the ideal horizontal extent of a LES domain shall be about two to three times the PBL height to allow for a correct development of horizontal convective cells, whose size scales like the PBL. In the vertical, the model uses 151 vertical levels from the surface to a model top at 8 km, which ensures that the vertical resolution is close to the horizontal grid spacing.

Each horizontal grid point in the LES model is initialized with the same vertical temperature profile extracted from the Mars Climate Database (MCD) at the targeted season and location for LES (Millour et al. 2015). A "background" horizontal wind of 10 m/s is imposed to simulate the influence of a regional-scale circulation, which tends to slightly enhance the daytime PBL turbulence and move convective cells and vortices towards a preferred direction in Martian plains (e.g. Reiss et al. 2014). The site chosen to carry out LES in this study is the InSight landing site E09 (latitude 4.4°N, longitude 136°E, altimetry -2652.6 m, albedo 0.26, thermal inertia 260 $\mathrm{J\,m^{-2}\,K^{-1}\,s^{-1/2}}$). Simulations are started at 07:00 local time at the (initially planned) landing season $Ls = 231.2°$ (northern fall). Following the report of the InSight mission, decided at the time of writing, the landing site will remain the same, but the landing season will change to $Ls = 19°$ (northern spring). However, the results presented in this paper are essentially left unaltered by this change of landing season, given the equatorial position of the InSight landing site. This is confirmed by the diurnal cycle of surface temperature simulated by the MCD at the InSight landing site, along with estimates of PBL depth obtained by the thermal plume parameterization described in Colaïtis et al. (2013).

An example of a dust-devil-like convective vortex resolved by the above-described Large-Eddy Simulations is shown in Fig. 10. This vortex is typical of the many vortices that arise in the simulations as the PBL convection develops during the day. Surface pressure and horizontal wind perturbations induced by this vortex are in agreement with the values acquired on Mars in situ (Schofield et al. 1997) and from orbit (Choi and Dundas

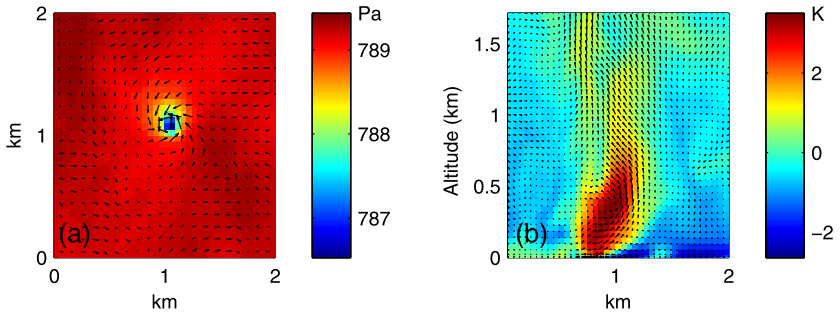

Fig. 10 A dust devil-like vortex as appearing in Large-Eddy Simulations. (**a**) Surface pressure and horizontal wind field. (**b**) Vertical section of temperature anomaly and wind field. In both cases the background horizontal wind of 10 m/s has been subtracted, to retain the tangential wind induced by the vortex itself

2011). The vertical section in Fig. 10 shows that the vertical extent of a typical dust devil is also well reproduced by LES. It is worth emphasizing here that the size of the vortex resolved in our 50 m LES are amongst the largest sizes observed on Mars, and that dust devils with a diameter less than 100 m are not resolved by our model.

Such limitation implies further developments, as most of the dust devils expected to occur at the InSight landing site areas are smaller than 10 m in diameter (Reiss and Lorenz 2016). However, resolving the smallest dust-devil-like perturbations is not essential to this study whose goals are to pave the way for future, higher resolution but more processing demanding analysis: here we aim at computing what will be the typical seismic signatures of dust devils on Mars by using a realistic time evolution of the three-dimensional pressure and wind fields. How the repeated seismic records acquired on Mars by SEIS could help to work out the complete statistics of dust devils (from largest to smallest vortices) is left for a future study in which 10-m-horizontal-resolution LES will be necessary.

4.2 Long-Period Seismic Signals

Coupling the results of the LES simulations with the theory described in Sect. 2.1, we obtained the seismometer accelerations induced by pressure disturbances for the two Mars subsurface models. An example of the LES pressure distribution and of the corresponding acceleration fields for the Regolith subsurface Model 1 is showed in Fig. 11. The pressure field includes two vortices of different sizes and with pressure drops of 0.7 and 1.6 Pa, respectively. The regions of highest vertical and horizontal accelerations coincide with vortices. However the influence zone of a vortex on the horizontal components is larger than on the vertical one (Fig. 11, (b) compared to (c) and (d)). Moreover, the amplitude of the acceleration fields, together with the distribution of the positive and negative acceleration poles, indicates that the main effect is related to ground tilt, as expected.

To visualize the distribution of vortices and other convective features and their seismic signal, movies are available as supplementary material. The simulation covering the daytime from 10 am to 4 pm (local time) shows the development and the collapse of the PBL and the formation of several dust devils, the most intense episodes being concentrated during the central hours (Online Resource 1). In the case of the regolith subsurface model, the corresponding seismic accelerations are shown on the horizontal (Online Resources 2 and 3) and vertical (Online Resource 4) component. The results indicate the level of the background noise induced by pressure fluctuations (see also Murdoch et al. 2017b) as well as the significant emergence of localized phenomena, such as atmospheric vortices.

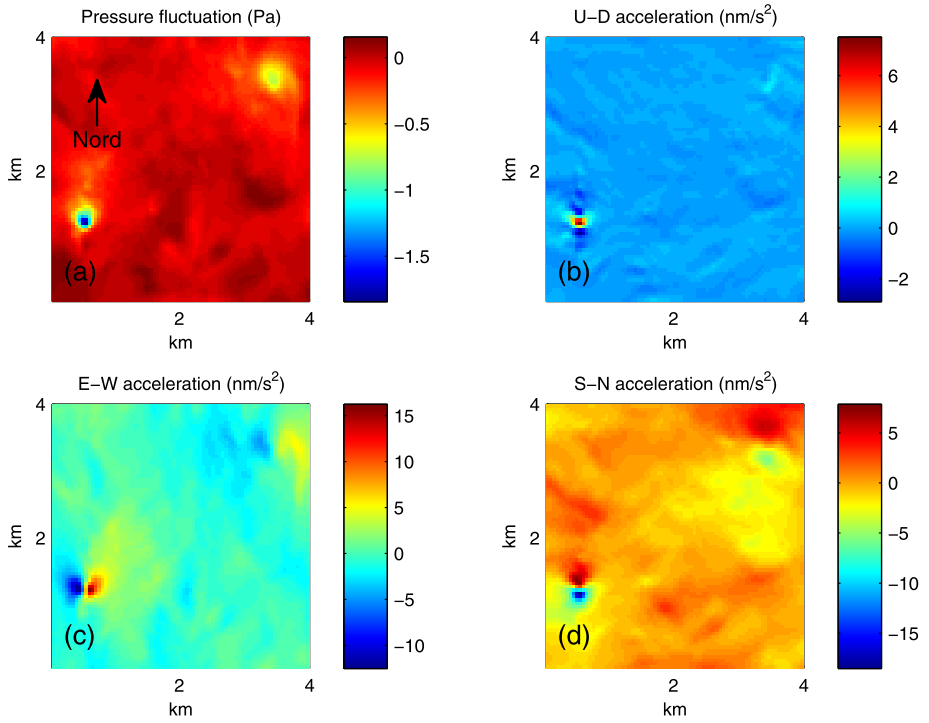

Fig. 11 Model of the long-period signals generated by the core-pressure drop of two different dust devil-like vortices. (**a**) Surface pressure drop from LES. (**b**) Vertical, (**c**) East-West and (**d**) South-North seismometer accelerations. The mean wind advecting the vortices is directed towards the North

The results of the modeling based on the full two-dimensional field of the LES can be compared to the local plane wave model derived from Sorrells' theory. The latter approach consists in convoluting the pressure time series P with the ground transfer function to retrieve the vertical displacement, and hence compute vertical acceleration and ground tilt in the S-N direction, i.e. in the direction of the background wind. Figure 12 shows the time-series of pressure, vertical and horizontal acceleration (for the regolith subsurface model) at distinct points during the passage of a vortex. The points are aligned orthogonally to the background wind and the distance between two consecutive points is of 150 m. The pressure fluctuation is clearly visible on two of the five time-series (Fig. 12a), in correspondence to the vortex core, whereas the seismic signal appears on at least four of them. The agreement between the results of the two methods is remarkable both on the vertical and on the S-N component (Figs. 12c and 12d, respectively). The waveforms are well reproduced and the difference in amplitude, particularly visible on the tilt data, is likely due to the complexity of the pressure field compared to its one-dimensional approximation in the Sorrells' approach. Nevertheless, the simple Sorrells' description gives the horizontal acceleration only in the background wind direction, therefore no comparison of the W-E waveforms is possible. In the case of atmospheric vortices advected by a background wind, the Sorrells' modeling seems to reproduce well the measured modeling and could be a simple but useful technique in the analysis of single-station data.

As a second application of our modeling, we computed the spectral ratio between the tilt and the pressure time series. This was first performed by Sorrells et al. (1971) and then

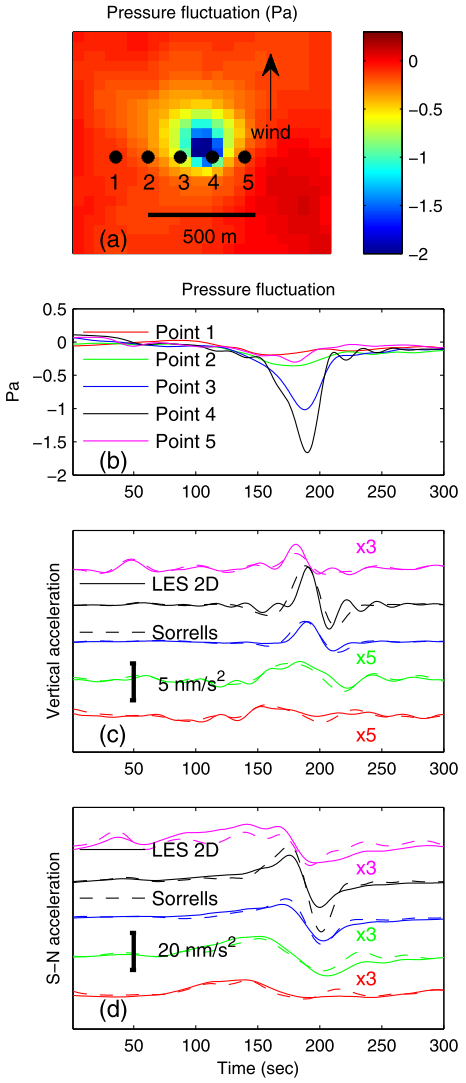

Fig. 12 Signature of a dust devil at distinct points on a cross section. (**a**) Position of the five points in a snapshot of the vortex pressure field. (**b**) Time history of the pressure fluctuations. (**c**) Comparison between the spectral computation (*continuous line*) and the Sorrells' approximation obtained by convolution of the pressure time history with the ground transfer function (*dashed line*) for the vertical component of the acceleration; the *colors* identify the points. (**d**) Same as (**c**) but for the S-N horizontal component of seismic acceleration, parallel to the background wind velocity

widely used to retrieve the compliance of the ground, especially in submarine seismology. The advantage of considering ground tilt instead of vertical velocity is that the former does not depend, in the modeling, on the wind velocity, which is often difficult to constrain precisely. We calculated the spectral ratio at different grid-points to mimic longer time series and obtain solid statistics. A total of about 200 time intervals of one-hour duration were considered and the corresponding ground response is shown in Fig. 13 for the two subsurface models. In the band 30–100 s, the mean of the apparent ground response compares well with the theoretical values; however, an overestimation of about 20% in the theoretical response appears for both models. Once again, the discrepancy is related to the fact that the theoretical model, based on Sorrells' response, does not account for the full complexity of the pressure field. Nevertheless, these results are encouraging for the use of long-period "noise" to retrieve the structure of the subsurface. In the case presented here, the data would

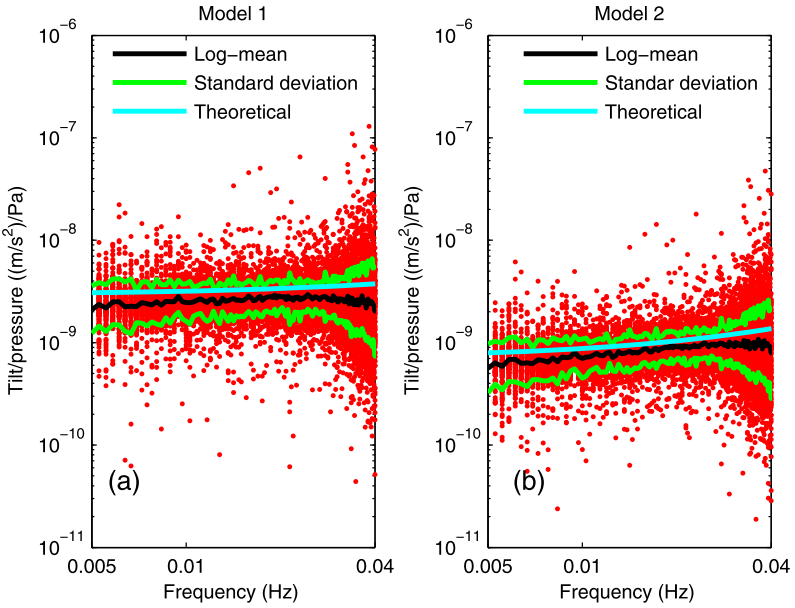

Fig. 13 Ground response to surface pressure loading. Each *red dot* corresponds to a measured value and the *black* and *green curves* are the log-mean and the standard deviation, respectively. The theoretical value in Sorrells' approximation is shown in *cyan*. (**a**) is for the purely regolith model, (**b**) for the subsurface model including a rocky layer

allow to distinguish between the subsurface structure below a few tens of meters depth, and shorter period data, down to a few seconds, would likely permit to estimate the compliance of the regolith.

We analyzed the three component of the seismic acceleration in correspondence to the passage of dust devils and compared the amplitude of the signal to the expected noise level. The synthetic time series (Fig. 14a), made for a dust devil generating a 2 Pa depression and the rocky subsurface model, show that the tilt effect is well above the noise level, provided the vortex is close enough to the receiver (for further discussion on this point cf. next paragraph). The vertical acceleration is instead typically at the limit of the self-noise level of the Very-Broad Band seismometer, and likely below the full system noise integrating the other noise sources. In the simple case of a dust devil propagating on a straight line aligned with one of the two horizontal axes of the seismometer, the two horizontal waveforms are slightly different from another: in the longitudinal direction the sign of the tilt acceleration changes, whereas in the transversal direction it does not. In intermediate cases the waveform analysis still permits to determine the azimuth of the dust devil migration, which does not directly result from single-point atmospheric measures.

An additional important point is to quantify how far a vortex can be detected by ground tilt: the decrease of the vertical and horizontal accelerations with distance is shown in Fig. 14b for the two reference subsurface models. The vertical signal decreases very rapidly for both models: a power-law adjustment indicates a $1/r^2$ behavior, r being the distance to the vortex center. Therefore, the vertical acceleration is practically significant only within the vortex itself, that is, only if the vortex passes precisely over the receiver. The horizontal acceleration scales instead as $1/r$ for $r > r_0$, r_0 being the radius of the vortex wall. The precise critical distance for the ground-tilt detection depends upon the ground compliance and

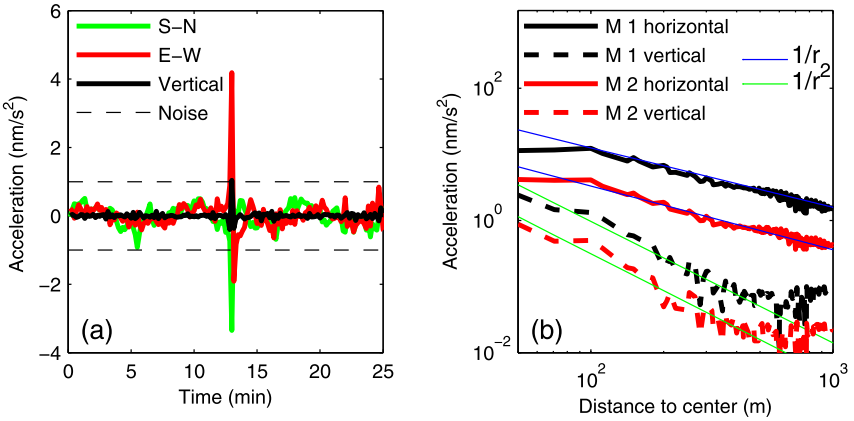

Fig. 14 Synthetic ground accelerations induced by a dust devil vortex with 2 Pa core-pressure drop. (**a**) Time series 50 m away from the vortex wall for the subsurface Model 2. (**b**) Decrease with distance of ground tilt (*continuous line*) and vertical acceleration (*dashed line*) for the two reference subsurface models; best fit power laws of $1/r$ (*blue*) and $1/r^2$ (*green*)

upon the pressure drop of the vortex. For the typical episode with 2 Pa core-pressure drop presented in Fig. 14b, the core radius is of 100 m, corresponding to the tilt maximum, and the detection limit is of a few hundreds meters for the rocky Model 2 and reaches 500–600 m for the regolith Model 1. The detection limit is in this case estimated based on the instrumental noise, i.e. 1 nm/s^2, and the background pressure noise, which is larger for Model 1.

4.3 Vortex Detection Statistics

Diurnal high-resolution LES simulations are used to estimate the occurrence of convective vortices at the InSight landing site. The LES carried out for this study are not capable of resolving all the small vortices expected on Mars. A complete statistic of the episodes requires challenging ultra-high-resolution LES (Nishizawa et al. 2016, see also the review by Spiga et al. 2016) which are beyond the scope of the present paper. Nonetheless, the 50-m-resolution LES employed in this study provide a self-consistent modeling for the largest vortices and the derived occurrence rates, if not realistic, can be considered as lower bounds. Moreover, the results of these simulations can be compared to the available ground-based and orbital data, helping with their interpretation and extrapolation. We first identified the vortices appearing over the whole domain during the day of the simulation and compared them to estimates of the dust devil frequencies coming from the analysis of dust devil tracks. After that, we computed the expected frequency with local time for a single station and compared our results with the meteorological data from previous missions to Mars.

Daily Detection Estimates We identified all the vortices appearing in the LES reference simulation with pressure drops of at least 0.5 Pa. We found 430 different episodes during a sol over the 14.4 km by 14.4 km area covered by the simulation: the cumulative frequencies per km^2 per sol are shown as functions of the maximal core pressure drop and of the diameter of the vortex in Fig. 15a. For each episode of the previous list, we also computed the maximal ground tilt acceleration for the two subsurface models (Fig. 15b).

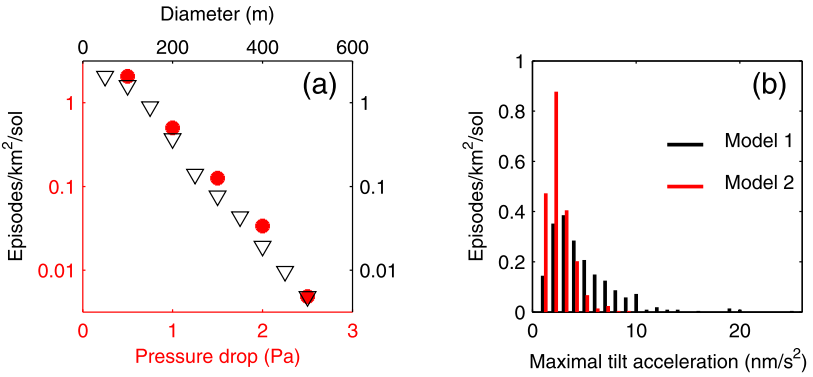

Fig. 15 Encounter frequency of vortices in the LES simulation. (**a**) Cumulative distribution in terms of maximal pressure drop (*red disks*) and diameter (*black triangles*). (**b**) Binned frequency as a function of maximal ground tilt for the two subsurface models

Observational indications of dust devil activity on Mars are provided by orbital imaging of the area. Vortices may indeed remove the fine layer of bright dust and expose the darker material underneath. Moreover a relationship between the diameter and the longevity of the vortices allows a comparison between orbital observations and single-station measurements or estimates at the surface (Lorenz 2013). For the InSight landing site, Reiss and Lorenz (2016) suggest a rate of 0.02–0.08 tracks/km^2/sol, with mean track width and length of 4 m and 600 m, respectively. We find similar occurrence rate for vortices with pressure drops of 1.75–2 Pa. However a direct comparison of these observations with the results of our modeling is difficult: LES with a horizontal resolution of 50 m do not resolve the small vortices appearing in orbital images and moreover they do not account for the lifting of dust.

The threshold for dust lifting on Mars is indeed poorly constrained: laboratory experiments in Martian conditions (Neakrase et al. 2006) and a Monte Carlo model proposed by Lorenz (2014) suggest a threshold of about 10–20 Pa, which is larger than the values measured on Mars by previous missions, or obtained in LES simulations. The possibility of such an intense event cannot be discarded even if its probability would be low. At the InSight landing site, we thus expect a full hierarchy of vortex events. Boundary layer vortices will surely be present, and a subset of these will be detected with the Very-Broad Band seismometer and some of these also through their pressure signature. Yet the majority of these events may be invisible, only a subset may actually lift dust to form dust devils with a detectable optical contrast, and only a subset of those may form trails.

Encounter Frequency with Local Time To analyze the diurnal variation, we computed the encounter frequency of convective vortices during one-hour time intervals. To do this, we evaluated the occurrence rate at each grid point during 60-min windows and we summed up and normalized the result with respect to the grid size. This approach allowed us to obtain statistics with a single-day LES (a simulation covering e.g. the whole mission duration being hardly realizable) and its validity relies on the ergodic hypothesis (see e.g. Galanti and Tsinober 2004). For each one-hour time series and for each grid point we defined detectable any episode with rapidly varying pressure or tilt signals (requiring a pressure drop of at least 0.5 Pa and a tilt acceleration of 5 nm/s^2, respectively). No false positive were identified among the automatically detected vortices; a more careful analysis of real data could however result in the detection of episodes with lower signal-to-noise ratio.

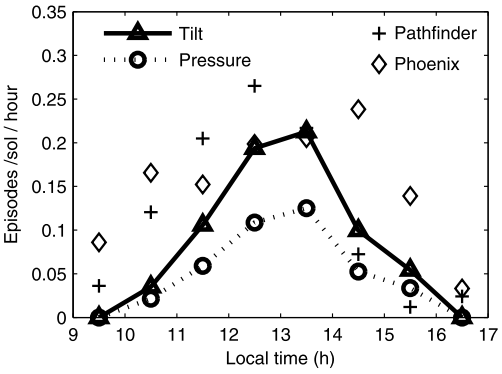

Fig. 16 Encounter frequency of convective vortices per sol per hour, by means of pressure fluctuation (*dotted line*) and ground tilt (*continuous line*). Results are for one sol with ambient wind at 10 m/s and the regolith subsurface model. The results for the Pathfinder and Phoenix missions are taken from Murphy and Nelli (2002) and Ellehoj et al. (2010), respectively

The diurnal variation of the encounter frequency is plotted in Fig. 16: according to this estimate, we can expect the SEIS, the APSS and Temperature and Wind sensor for InSight (TWINS) experiments to routinely detect atmospheric vortices in the central hours of the day. Moreover, this probability is actually a lower limit since many small-size dust devils—typically 10 m in diameter—are not resolved by the 50 m LES described in this paper. This limitation accounts for our values being smaller than the detection rates of convective vortices with the same threshold of 0.5 Pa by the Pathfinder and Phoenix meteorological experiments, shown for comparison in Fig. 16. Although atmospheric vortices form even in absence of environmental wind, the probability of detection depends on the mean wind speed: indeed vortices are advected by the mean wind and cover therefore a larger area. The probability values also show that the seismometer may be capable of detecting remote encounters, i.e. vortices not directly appearing in the pressure records, as previously argued by Lorenz et al. (2015) in relationship to the seismometer detection of terrestrial dust devils.

5 Conclusion

Numerical modeling of local atmospheric turbulence and of the seismic signal it generates suggests that the SEIS experiment could detect the passage of atmospheric vortices and dust devils by ground tilt. The amplitude of the signal depends on the source—mainly on the pressure drop and on the missing distance—and on the ground response to static loading. A characterization of the source can be performed through the analysis of the APSS/TWINS pressure and wind-velocity data and possibly through the orbital identification of the surface track of intense dust devil episodes. The long-period seismic data may as well include vortex-induced signals: these would help in detemine the properties of the source (migration direction) and of the near surface structure through the spectral ratio of seismic and pressure records, as discussed above. Moreover, techniques based on single-station data, such as Sorrells' theory, appear to fit the vortex-induced signal, both on Mars synthetics and Earth data, and may thus be used in the investigation. The seismic short-period excitation and the infrasound recorded during a vortex event also carry powerful information about the missing distance on the one hand, and about the propagation of shallow surface waves on the other hand.

In the case atmospheric vortices are detected, a joint analysis of seismic and atmospheric data is thus expected to lead us to: (1) describe the excitation source; (2) estimate the compliance of the regolith, and possibly of harder underlying layers, at the InSight landing site

through the long-period seismic response to the pressure loading; (3) obtain additional constraint on the near-surface structure, through the propagation characteristic of shallow surface waves. In addition to the subsurface exploration at the InSight landing site, the analysis of atmospheric vortices will result in a better characterization of the dynamics of the PBL and, in the case of dust devils, of the eolian transport in the atmosphere of Mars.

Acknowledgements This work has been supported by CNES and ANR SismoMars in the frame of the preparation of InSight/SEIS. B. Kenda acknowledges the support of ED560 STEP'UP and of the NASA InSight project for his PhD support. R. Lorenz acknowledges the support of NASA Grant NNX12AI04G. Research described in this paper was partially done by the InSight Project, Jet Propulsion Laboratory, California Institute of Technology, under a contract with the National Aeronautics and Space Administration. This is IPGP contribution 3844. This is InSight Contribution Number 26. We gratefully thank the Editor and two anonymous reviewers, whose comments helped us in improving the manuscript.

References

H. Arai, K. Tokimatsu, S-wave velocity profiling by inversion of microtremors H/V spectrum. Bull. Seismol. Soc. Am. **94**, 53–63 (2004)

R. Beauduin, P. Lognonné, J.P. Montagner, S. Cacho, J.F. Karczewski, M. Morand, The effects of the atmospheric pressure changes on seismic signals or how to improve the quality of a station. Bull. Seismol. Soc. Am. **86**, 1760–1769 (1996)

A.J. Bedard, Low-frequency atmospheric acoustic energy associated with vortices produced by thunderstorms. Mon. Weather Rev. **133**, 241–263 (2005)

S. Bonnefoy-Claudet, A. Köhler, C. Cornou, M. Wathelet, P.-Y. Bard, Effect of love waves on microtremor H/V ratio. Bull. Seismol. Soc. Am. **98**, 288–300 (1998)

D.S. Choi, C.M. Dundas, Measurements of Martian dust devils winds with HiRISE. Geophys. Res. Lett. **38**, L24206 (2011)

A. Colaïtis, A. Spiga, F. Hourdin, C. Rio, F. Forget, E. Millour, A thermal plume model for the martian convective boundary layer. J. Geophys. Res. **118**, 1468–1487 (2013)

P. Delage, F. Karakostas, A. Dhemaied, Y.J. Cui, M.D. Laure, The geotechnical properties of some Martian regolith simulants in link with the InSight landing site. Space Sci. Rev. (2017, this issue). doi:10.1007/s11214-017-0339-7

M.D. Ellehoj, H.P. Gunnlaugsson, P.A. Taylor, H. Kahanpää, K.M. Bean, B.A. Cantor, B.T. Gheynani, L. Drube, D. Fischer, A.-M. Harri, C. Holstein-Rathlou, M.T. Lemmon, M.B. Madsen, M.C. Malin, J. Polkko, P.H. Smith, L.K. Tamppari, W. Weng, J. Whiteway, Convective vortices and dust devils at the Phoenix Mars mission landing site. J. Geophys. Res. **115**, E00E16 (2010)

W.M. Farrell, P.H. Smith, G.T. Delory, G.B. Hillard, J.R. Marshall, D. Catling, M. Hecht, D.M. Tratt, N. Renno, M.D. Desch, S.A. Cummer, J.G. Houser, B. Johnson, Electric and magnetic signatures of dust devils from the 2000–2001 MATADOR desert tests. J. Geophys. Res. **109**, E03004 (2004)

B. Galanti, A. Tsinober, Is turbulence ergodic? Phys. Lett. A **330**, 173–180 (2004)

M. Golombek, D. Kipp, N. Warner, I.J. Daubar, R. Fergason, R. Kirk, R. Beyer, A. Huertas, S. Piquex, N. Putzig, B.A. Campbell, G.A. Morgan, C. Charalambous, W.T. Pike, K. Gwinner, F. Calef, D. Kass, M. Mischna, J. Ashley, C. Bloom, N. Wigton, C. Schwartz, H. Gengl, L. Redmond, J. Sweeney, E. Sklyanskiy, M. Lisano, J. Bernardino, P. Lognonné, S. Smrekar, B. Banerdt, Selection of the InSight landing site. Space Sci. Rev. (2017, this issue). doi:10.1007/s11214-016-0321-9

R.B. Herrmann, Computer programs in seismology: an evolving tool for instruction and research. Seismol. Res. Lett. **84**, 1081–1088 (2013)

D.P. Hinson, M. Patzold, S. Tellmann, B. Häusler, G.L. Tyler, The depth of the convective boundary layer on Mars. Icarus **198**, 57–66 (2008)

M.S. Howe, Lectures on the theory of vortex sound, in *Sound-Flow Interactions*, ed. by Y. Aurégan, A. Maurel, V. Pagneux, J.-F. Pinton (Springer, Berlin, 2002), pp. 31–110

H. Kahanpää, C. Newman, J. Moores, M.-P. Zorzano, J. Martín-Torres, S. Navarro, A. Lepinette, B. Cantor, M.T. Lemmon, P. Valentín-Serrano, A. Ullán, W. Schmidt, Convective vortices and dust devils at the MSL landing site: annual variability. J. Geophys. Res., Planets (2004). doi:10.1002/2016JE005027

S. Kedar, J. Andrade, B. Banerdt, P. Delage, M. Golombek, T. Hudson, A. Kiely, M. Knapmeyer, B. Knapmeyer-Endrun, C. Krause, T. Kawamura, P. Lognonné, T. Pike, Y. Ruan, N. Teanby, J. Tromp, J. Wookey, Analysis of regolith properties using seismic signals generated by InSights HP3 penetrator. Space Sci. Rev. (2017, this issue)

B.L.N. Kennet, *Seismic Waves Propagation in Stratified Media* (Cambridge University Press, Cambridge, 1983)
B. Knapmeyer-Endrun, M.P. Golombek, M. Ohrnberger, Rayleigh wave ellipticity modeling and inversion for shallow structure at the proposed InSight landing site in Elysium Planitia, Mars. Space Sci. Rev. (2017, this issue). doi:10.1007/s11214-016-0300-1
K. Konno, T. Ohmachi, Ground-motion characteristic estimated from spectral ratio between horizontal and vertical components of microtremors. Bull. Seismol. Soc. Am. **88**, 228–241 (1998)
E. Larose, A. Khan, Y. Nakamura, M. Campillo, Lunar subsurface investigated from correlation of seismic noise. Geophys. Res. Lett. **32**, L16201 (2005)
D.K. Lilly, On the numerical simulation of buoyant convection. Tellus **14**, 148–162 (1962)
P. Lognonné, B. Mosser, Planetary seismology. Surv. Geophys. **14**, 239–302 (1993)
P. Lognonné, J. Gagnepaine Beyneix, W.B. Banerdt, S. Cacho, J.F. Karxzewski, M. Moran, Ultra broad band seismology on InterMarsNet. Planet. Space Sci. **44**, 1241–1249 (1996)
P. Lognonné, C. Johnson, Planetary seismology, in *Treatise in Geophysics, Volume 10: Planets and Moons*, ed. by G. Schubert (Elsevier, Amsterdam, 2007), pp. 67–122
P. Lognonné, W.T. Pike, Planetary seismometry, in *Extraterrestrial Seismology*, ed. by V.C.H. Tong, R.A. García (Cambridge University Press, Cambridge, 2015), pp. 36–50
R.D. Lorenz, Obseving desert dust devils with a pressure logger. Geosci. Instrum. Method. Data Syst. **1**, 209–220 (2012)
R.D. Lorenz, The longevity and aspect ratio of dust devils: effects on detection efficiencies and comparison of landed and orbital imaging at Mars. Icarus **226**, 964–970 (2013)
R.D. Lorenz, Vortex encounter rates with fixed barometer stations: comparison with visual dust devil counts and large eddy simulations. J. Atmos. Sci. **71**, 4461–4472 (2014)
R.D. Lorenz, D. Christie, Dust devil signatures in infrasound records of the international monitoring system. Geophys. Res. Lett. **42**, 2009–2014 (2015)
R.D. Lorenz, S. Kedar, N. Murdoch, P. Lognonné, T. Kawamura, D. Mimoun, W.B. Banerdt, Seismometer detection of dust devil vortices by ground tilt. Bull. Seismol. Soc. Am. **105**, 3015–3023 (2015)
R.D. Lorenz, M.R. Balme, Z. Gu, H. Kahanpää, M. Klose, M. Kurgansky, M.R. Patel, D. Reiss, A.P. Rossi, A. Spiga, T. Takemi, W. Wei, History and applications of dust devil studies. Space Sci. Rev. **203**, 5–37 (2016)
P.G. Malischewsky, F. Scherenbaum, Love's formula and H/V-ratio (ellipticity) of Rayleigh waves. Wave Motion **40**, 57–67 (2004)
P.J. Mason, Large-eddy simulation of the convective atmospheric boundary layer. J. Atmos. Sci. **46**, 1492–1516 (1989)
T.I. Michaels, S.C.R. Rafkin, Large-eddy simulation of atmospheric convection on Mars. Q. J. R. Meteorol. Soc. **130**, 1251–1274 (2004)
E. Millour, F. Forget, A. Spiga, T. Navarro, J.-B. Madeleine, L. Montabone, A. Pottier, F. Lefevre, F. Montmessin, J.-Y. Chaufray, M.A. Lopez-Valverde, F. Gonzalez-Galindo, S.R. Lewis, P.L. Read, J.-P. Huot, M.-C. Desjean, The Mars Climate Database (MCD version 5.2), EPSC (2015)
D. Mimoun, N. Murdoch, P. Lognonné, T. Pike, K. Hurst (the SEIS team), The seismic noise model of the InSight mission to Mars. Space Sci. Rev. (2017, this issue)
M. Mucciarelli, M.R. Gallipoli, D. Di Giacomo, F. Di Nota, E. Nino, The influence of wind on measurements of seismic noise. Geophys. J. Int. **161**, 303–308 (2005)
N. Murdoch, D. Mimoun, R.F. Garcia, W. Rappin, T. Kawamura, P. Lognonné, Evaluating the wind-induced mechanical noise on the InSight seismometers. Space Sci. Rev. (2017a, this issue). doi:10.1007/s11214-016-0311-y
N. Murdoch, B. Kenda, T. Kawamura, A. Spiga, P. Lognonné, D. Mimoun, W.B. Banerdt, Pressure noise on Mars determined from large-eddy simulations. Space Sci. Rev. (2017b, this issue). doi:10.1007/s11214-017-0343-y
J.R. Murphy, S. Nelli, Mars Pathfinder convective vortices: frequency of occurrence. Geophys. Res. Lett. **29**, 2103 (2002)
V. Naderyan, C.J. Hickey, R. Raspet, Wind-induced ground motion. J. Geophys. Res., Solid Earth **121**, 917–930 (2016)
L.D.V. Neakrase, R. Greeley, J.D. Iversen, M.R. Balme, Dust flux within dust devils: preliminary laboratory simulations. Geophys. Res. Lett. **33**, L19S09 (2006)
F.M. Neubauer, Thermal convection in the Martian atmosphere. J. Geophys. Res. **71**(10), 2419–2426 (1966)
S. Nishizawa, M. Odaka, Y.O. Takahash, K. Sugiyama, K. Nakajima, M. Ishiwatari, S. Takehiro, H. Yashiro, Y. Sato, H. Tomita, Y.-Y. Hayashi, Martian dust devil statistics from high-resolution large-eddy simulations. Geophys. Res. Lett. **43**, 4180–4188 (2016)
S.C.R. Rafkin, R.M. Haberle, T.I. Michaels, The Mars regional atmospheric modeling system: model description and selected simulations. Icarus **151**, 228–256 (2001)

D. Reiss, R.D. Lorenz, Dust devil track survey at Elysium Plmanitia: implications for the InSight landing sites. Icarus **266**, 315–330 (2016)
D. Reiss, A. Spiga, G. Erkeling, The horizontal motion of dust devils on Mars derived from CRISM and CTX/HiRISE observations. Icarus **227**, 8–20 (2014)
N.O. Rennó, A.A. Nash, J. Lunine, J. Murphy, Martian and terrestrial dust devils: test of a scaling theory using Pathfinder data. J. Geophys. Res. **105**, 1859–1865 (2000)
N.O. Rennó, V.J. Abreu, J. Koch, P.H. Smith, O.K. Hartogensis, H.A.R. De Bruin, D. Burose, G.T. Delory, W.M. Farrell, C.J. Watts, J. Garatuza, M. Parker, A. Carswell, MATADOR 2002: a pilot field experiment on convective plumes and dust devils. J. Geophys. Res. **109**, E07001 (2004)
M.H. Ritzwoller, A.L. Levshin, Estimating shallow shear wave velocities with marine multicomponent seismic data. Geophysics **67** (2002). doi:10.1190/1.1527099
J.A. Ryan, R.D. Lucich, Possible dust devils, vortices on Mars. J. Geophys. Res. **88**(C15), 11005–11011 (1986)
E.D. Schmitter, Modeling tornado dynamics and the generation of infrasound, electric and magnetic field. Nat. Hazards Earth Syst. Sci. **10**, 295–298 (2010)
J.T. Schofield, J.R. Barnes, D. Crisp, R.M. Haberle, S. Larsen, J.A. Magalhaes, J.R. Murphy, A. Seiff, G. Wilson, The Mars Pathfinder Atmospheric Structure Investigation/Meteorology (ASI/MET) experiment. Science **278**(5344), 1752–1758 (1997)
W.C. Skamarock, J.B. Klemp, A time-split nonhydrostatic atmospheric model for weather research and forecasting applications. J. Comput. Phys. **227**, 3465–3485 (2008)
G.G. Sorrells, A preliminary investigation into the relationship between long-period seismic noise and local fluctuations in the atmospheric pressure field. Geophys. J. R. Astron. Soc. **26**, 71–82 (1971)
G.G. Sorrells, J.A. McDonald, Z.A. Der, E. Herrin, Earth motion caused by local atmospheric pressure changes. Geophys. J. R. Astron. Soc. **26**, 83–98 (1971)
A. Spiga, F. Forget, A new model to simulate the Martian mesoscale and microscale atmospheric circulation: Validation and first results. J. Geophys. Res., Planets **114** (2009). doi:10.1029/2008JE003242
A. Spiga, F. Forget, S.R. Lewis, D.P. Hinson, Structure and dynamics of the convective boundary layer on Mars as inferred from large-eddy simulations and remote-sensing measurements. Q. J. R. Meteorol. Soc. **136**, 414–428 (2010)
A. Spiga, E. Barth, Z. Gu, F. Hoffmann, J. Ito, B. Jemmett-Smith, M. Klose, S. Raasch, S. Rafkin, T. Takemi, D. Tyler, W. Wei, Large-eddy simulations of dust devils and convective vortices. Space Sci. Rev. **203**, 245–275 (2016)
F.B. Tatom, K.R. Knupp, S.J. Vitton, Tornado detection based on seismic signal. J. Appl. Meteorol. **34**, 572–582 (1995)
A.D. Toigo, M.I. Richardson, S.P. Ewald, P.J. Gierasch, Numerical simulation of Martian dust devils. J. Geophys. Res. **108**, 95 (2003)
G.H. Vatistas, V. Kozel, W.C. Mih, A simpler model for concentrated vortices. Exp. Fluids **11**, 73–76 (1991)
N.H. Warner, M.P. Golombek, J. Sweeney, R. Fergason, R. Kirk, C. Schwartz, Near surface stratigraphy and regolith production in southwestern Elysium Planitia, Mars: implications for Hesperian-Amazonian terrains and the InSight lander mission. Space Sci. Rev. (2017, this issue). doi:10.1007/s11214-017-0352-x
M.M. Withers, R.C. Aster, C.J. Young, E.P. Chael, High-frequency analysis of seismic background noise as a function of wind speed and shallow depth. Bull. Seismol. Soc. Am. **86**, 1507–1515 (1996)
W. Zürn, J. Exss, H. Steffen, C. Kroner, T. Jahr, M. Westerhaus, On reduction of long-period horizontal seismic noise using local barometric pressure. Geophys. J. Int. **171**, 780–796 (2007)